Research Article | Vol. 30, No. 9 / 25 Apr 2022 / Optics Express 15766
Optics EXPRESS

Compact and high Q-factor multimode racetrack ring resonator based on transformation optics

LIFENG CAI,[1] DINGSHAN GAO,[1,*] JIANJI DONG,[1] JIN HOU,[2] CHUNYONG YANG,[2] SHAOPING CHEN,[2] AND XINLIANG ZHANG[1]

[1]*Wuhan National Laboratory for Optoelectronics & School of Optical and Electronic Information, Huazhong University of Science and Technology, 1037 Luoyu Road, Wuhan 430074, China*
[2]*Hubei Key Laboratory of Intelligent Wireless Communications, College of Electronics and Information Engineering, South-Central University for Nationalities, Wuhan 430074, China*
[*]*dsgao@hust.edu.cn*

Abstract: The ring resonator is a versatile and functional component in the silicon-based integrated optical circuit. Most of the previously reported ring resonators work in the single-mode case. With the rapid development of mode division multiplexing technology, a multimode ring resonator (MMRR) has been proposed and the usage beyond the limit of a conventional single mode ring resonator has been explored. However, the reported MMRRs are either large in size or low in quality factor. In this paper, we designed a compact silicon MMRR with a small bending radius of 15μm, in which the three lowest TE modes all have high Q-factors. For suppressing the mode loss and inter-mode crosstalk in MMRR, a multimode waveguide bend (MWB) with mode adiabatic evolution was designed based on transformation optics and waveguide shape optimization. The independent excitation of each order mode of the MMRR is realized by using bending directional coupler and asymmetric directional coupler. We successfully fabricated the device on a silicon-on-insulator (SOI) platform using simple one-step lithography. The measured loaded Q-factors of the three lowest TE modes are 5.9×10^4, 4.5×10^4, and 4.7×10^4, respectively.

1. Introduction

Silicon photonics is a promising platform for constructing on-chip optical communication systems with low cost, high performance, and compatibility with complementary metal-oxide-semiconductor (CMOS) fabrication technologies [1,2]. Meanwhile, the silicon-on-insulator (SOI) platform has a large refractive index difference, which can realize compact silicon-based devices and high-density integrated photonics circuits [3]. In recent years, silicon photonics circuits utilizing multiplexing technologies on wavelength [4,5] and polarization [6,7] have been intensively demonstrated for on-chip optical communication. To further expand the transmission capacity and bandwidth, mode division multiplexing (MDM) is introduced [8,9]. For transmitting MDM signals, a series of multimode waveguide devices have been proposed, such as multimode bend [10], multimode crossing [11,12], and multimode splitter [13]. Furthermore, devices for multimode switching and routing have also been demonstrated [14,15].

Ring resonators play an important role in silicon photonics circuits due to their small size and diverse functions, which are widely used as modulators [16], filters [17], multiplexers [18], lasers [19], and sensors [20]. But traditional ring resonators mainly focus on single-mode operation, which is not compatible with the MDM system. The research on multimode ring resonator (MMRR) is becoming attractive for on-chip MDM systems. Moreover, the MMRR can be used in other novel applications, such as microwave photonic filters [21], OAM emitters [22], multiparameter optical sensors [23], and multimode nonlinear optics [24]. However, due to the loss of high-order modes and inter-mode crosstalk, it is still a great challenge to obtain a multimode ring resonator with a high Q value and excite each mode independently.

#457020 https://doi.org/10.1364/OE.457020
Journal © 2022 Received 23 Feb 2022; revised 9 Apr 2022; accepted 11 Apr 2022; published 22 Apr 2022

Optics EXPRESS

Previously, several methods for designing MMRRs have been proposed. In Ref. [25], four adiabatic Bezier curve 90° waveguide bends connecting with the straight waveguide are used to form an MMRR for two TE modes. The coupling region is optimized to realize the multiplexing of two modes. But expanding to support more modes needs a larger bending radius, which will shrink the free spectral range (FSR) severely. In addition, the FSRs of the two modes are quite different due to the large resonator length and the coupling region design, which will affect its application in practical systems. Another design method of MMRR for two modes is proposed in Ref. [26], in which two 180° modified Euler waveguide bends and a subwavelength grating (SWG) coupler are used. The SWG can enhance the coupling efficiency of each mode to decrease the coupling length but lead to high loss and inter-mode crosstalk. Meanwhile, the effective radius of Euler bending needs to be large enough to support more modes. In Ref. [27], an MMRR with four modes was proposed using the total internal reflection (TIR) from the waveguide sidewall mirror and the frustrated TIR coupling method. However, due to the scattering caused by the rough sidewall, the insertion loss of the device is large. The Q-factors of the four modes are low, only a few thousand.

In this paper, we propose and demonstrate a compact and high Q silicon MMRR supporting three modes, which consists of two multimode straight waveguides and two 180° multimode waveguide bends (MWBs) designed by transformation optics (TO). The proposed MWB is formed by optimizing the boundary shape of the device in the virtual space to realize mode adiabatic evolution between the straight waveguide modes and bend waveguide modes. The effective radius of the MWB is as small as 15 μm, which makes the MMRR very compact and has a large FSR. The MWB can be combined with a bending directional coupler (BDC) to stimulate the TE_0 mode in the resonator without exciting other modes. The selective coupling of TE_1 and TE_2 mode in the MMRR is realized by the asymmetrical directional coupler (ADC). With this design, each mode can be selectively excited and propagates in the MMRR with low loss and low inter-mode coupling. We fabricated the MMRR by E-beam lithography and single etching process on a commercial SOI wafer. The measured loaded Q-factors for TE_0, TE_1, and TE_2 modes are 5.9×10^4, 4.5×10^4, and 4.7×10^4 respectively, and the corresponding FSR is 3.7 nm, 3.6 nm, and 3.4 nm respectively. Our proposed compact and high Q MMRR has great potential in many applications, including on-chip MDM systems, microwave photonics, multi-parameter optical sensors, and multimode nonlinear optics.

2. Design and simulation of the multimode waveguide bend and ring resonator

Figure 1 is the schematic of the proposed silicon MMRR, which is based on two 180° MWBs connecting with two straight waveguides. The MMRR is designed on the commercial silicon-on-insulator (SOI) wafer with a 220 nm thick top silicon layer, and a 3 μm thick buried-oxide layer. The over cladding is 2 μm thick SiO_2, which is not shown in Fig. 1. To selectively excite the fundamental mode in the MMRR, a BDC is used on one MWB so that the mode coupling only happens between the fundamental modes in the narrow access waveguide and the wide MWB due to the bending phase matching. Two ADCs are designed for selectively coupling the fundamental mode in the narrow access waveguide with the TE_1 or TE_2 mode in the wide straight waveguide of MMRR. If the light is propagating through the connection between the straight waveguide and conventional arc-bend waveguide, significant losses and inter-mode crosstalk will be introduced due to the strong mode mismatching when the bending radius is not sufficiently large. Normally a very large bending radius is needed to achieve MMRR with high-Q factors for several modes. But achieving compact size and large FSRs by reducing the length of MMRR is highly demanded. To solve this problem, here we design a MWBs perfectly matched with the mode field of the straight waveguide based on shape optimization in the virtual space by the TO method. That is, the MWB can realize the adiabatic evolution of the mode field from multimode straight waveguide to multimode curved waveguide.

Optics EXPRESS

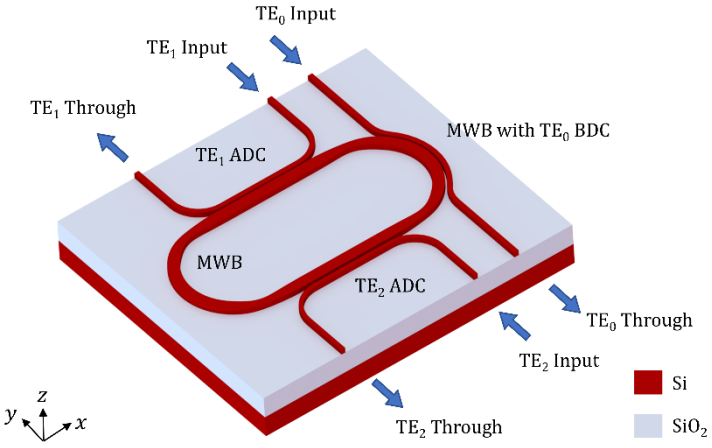

Fig. 1. Schematic configurations of the proposed high-Q multimode ring resonator.

TO [28,29] is a powerful design method to control the propagation of electromagnetic waves by using the coordinate transformation and obtaining the required permittivity and permeability distribution of the device. TO is a rigorous theory deriving from Maxwell's equations, which does not introduce too many approximations. This feature is important for accurately designing integrated optics device. Nonetheless, not only in the flexible general coordinate transformation [30] but also in the optical surface transformation [31–33], the usage of metamaterial is inevitable. It is hard to be realized in the optical regime and usually works in a narrow bandwidth with high loss. However, when the coordinate transformation is conformal mapping (CM), the device will be simplified to gradient index distribution without introducing complex anisotropic materials [34]. The distribution of refractive index after CM can be obtained by the equation $n' = n/\sqrt{\det(\mathbf{P})}$, where n is either the waveguide effective index or the cladding index, and $\mathbf{P}$ is the Jacobian matrix of CM.

To design a MWB, firstly we transform the 180° arc-bend waveguide including the cladding area into a straight waveguide. Because of the covariance of Maxwell's equations, the device performance remains the same before and after CM. The original arc-bend waveguide is in the physical space of (x, y) coordinates. While the transformed straight waveguide is in the virtual space of (u, v) coordinates. As shown in Fig. 2(a), the arc-bend waveguide is composed of an arc-bend with radius R = 10 μm and two extra straight waveguides with length L_a = 5 μm and width W_s =5 μm. These two extra straight waveguides are used for connecting with the input and output waveguide smoothly. Figure 2 (b) shows the straight waveguide in the virtual space after CM. The CM can be obtained by solving Laplace's equation setting on the arc-bend waveguide. The waveguide width remains unchanged by setting the boundary condition of the Laplace equation as v=-2.5 μm and v = 2.5 μm on the inner and outer arc boundaries of the arc-bend respectively. And the boundary conditions of u = 0 and u = L_t are set on the input and output ends of the arc-bend.

The width of transformation area W_s is chosen to be larger than the waveguide width due to two reasons. First, the evanescent field exists in the cladding area, which will affect the simulation performance of the device. Second, we need to provide enough space for shape variation of waveguide boundaries during the optimization process. And we find that setting W_s = 5 μm is enough for optimization. On the other hand, the parameter L_t is not set arbitrarily, otherwise the coordinate transformation will not be conformal. So L_t is indeed determined by the W_s but without an explicit expression. Thus, we use an optimization process to obtain the value of L_t by setting L_t as the optimization parameter and the Cauchy-Riemann condition as the optimization

Optics EXPRESS

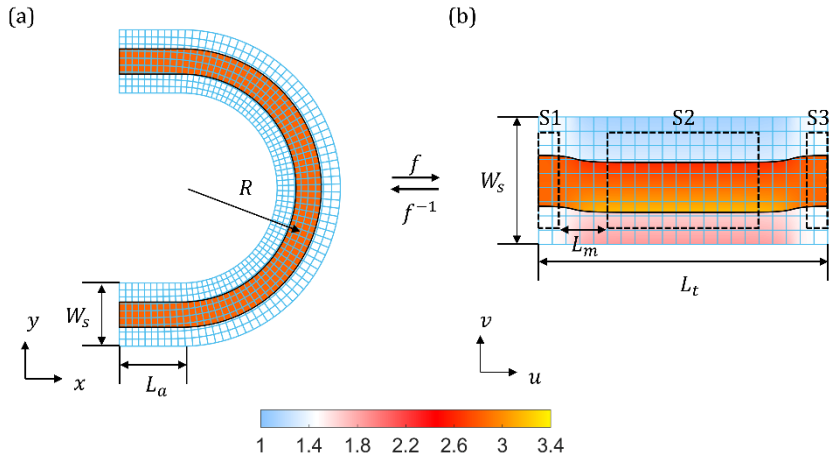

Fig. 2. The conformal mapping (CM) from an original arc-bend waveguide in physical space to a straight waveguide in virtual space. The color profile is the refractive index distribution of the waveguide including the cladding area. (a) The radius of the arc-bend is R = 10 μm. The length of the extra rectangle is L_a = 5 μm, and the width is W_s = 5 μm. (b) The width of the straight waveguide in the virtual space is W_s =5 μm. The length L_t is optimized to be L_t =40.778 μm, ensuring that u and v meet the Cauchy-Riemann condition of CM. For the three marked sections (S1, S2 and S3), the index distribution is translation invariant along the u direction.

objective. This CM can be calculated by combining the Laplace and optimization modules in the COMSOL Multiphysics software (http://www.comsol.com). After optimization process converges, we find that the optimal L_t is 40.778 μm and the area average of $|u_x/v_y$ -1| in the whole transformation area is below 5×10^{-7}. Therefore, the coordinate transformation is conformal. The details can be found in our previous work [35].

As shown in Fig. 2(b), the color profile is the refractive index distribution of the waveguide after CM including the cladding area. From the index distribution in virtual space, we can find two different types of area. In section S1, S2 and S3, the index only gradually changes along the cross-section direction and nearly keeps invariant along the propagation direction, which indicates the existence of stable guided modes. Relating with the physical space, the section S1 and S3 are parts of the original input and output straight waveguides, and the section S2 corresponds to part of arc-bend waveguide. In these sections, light propagates following the eigenmodes of the straight or curved waveguide. For the area between the section S1(S3) and S2 marked with the length of L_m in Fig. 2(b), the index changes gradually in both *u* and *v* directions. Normally, the straight waveguide modes are not able to convert to the curved waveguide mode adiabatically after passing through this area. Thus, we can find that the mode loss and crosstalk of traditional arc-bend waveguide arise from the non-adiabatic transition of eigenmodes. To obtain perfect multimode waveguide bending, we can use two mode converters among these sections to adiabatically transform each straight waveguide mode to the corresponding bend waveguide mode and then transform back. This mode converter can be directly designed by shape optimization in the virtual space.

Since the conformal mapping is implemented in a 2D plane, the simulation and shape optimization in the virtual space is also implemented in 2D plane. We use the effective index method to approximate the 3D waveguide to an equivalent 2D waveguide in x-y plane. The whole device is designed within a 220 nm thick silicon layer with upper and lower claddings of SiO_2, which can only support the fundamental mode of the slab waveguide with the equivalent

Optics EXPRESS

index of 2.84. The widths of the input straight waveguide and bending waveguide are set to be 2 μm to support the three lowest TE modes, which can also reduce the scattering loss from the sidewall roughness. The boundary curves of the mode converter can be expressed by the Fourier series, and the expressions of the upper and lower boundary curves v_1 and v_2 are

$$v_1 = a_0 + a_1\cos(wu) + a_2\cos(2wu) + a_3\sin(wu) + a_4\sin(2wu), \quad (1)$$

$$v_2 = b_0 + b_1\cos(wu) + b_2\cos(2wu) + b_3\sin(wu) + b_4\sin(2wu), \quad (2)$$

where $w = 2\pi/L_m$. Considering the shape of the mode converter maybe not symmetric, both the cosine and sine terms of the Fourier series are needed. Only two cosine and sine terms are used here to save optimization time without any obvious deterioration on the mode conversion performance. The parameters a_1, a_2, a_3, b_1, b_2, and b_3 are the optimization variables. Since the boundary curves of the mode converter need to be smooth, a_0, b_0, a_4, and b_4 can be determined by the optimization variables and the waveguide width. We set the transmission efficiency of each mode as the optimization objectives and set the inter-mode crosstalk as the optimization constraints. The optimization is realized by combing the 2D wave optics module with the "BOBYQA" method in the optimization module of the COMSOL Multiphysics software. The upper bound of the optimization constraints are all -25 dB. During the optimization process, the program inputs different modes in turn at different variables and calculates the transmission efficiency and the inter-mode crosstalks of each mode. The program will choose the lowest efficiency among the three modes as the result in each optimization cycle. When the optimization objectives are close to the predefined threshold, the optimization process converges and stops. The optimized parameters are $a_0 = 0.813685$, a_1=-0.205039, a_2=-0.018724, a_3=-0.065382, a_4=-0.032691, b_0=-0.914395, $b_1 = 0.104497$, $b_2 = 0.018891$, b_3=-0.026028 and b_4=-0.013014. Figure 3 (a)–(c) show the H_z field of TE_0, TE_1 and TE_2 mode propagating in the shape-optimized mode converter in the virtual space respectively, at the wavelength of 1550 nm. The eigenmodes between the straight waveguide and the bending waveguide can be converted adiabatically without any obvious scattering or crosstalk. The losses of the three lowest-order TE modes are all less than 0.01 dB, and the inter-mode crosstalks are all less than -25 dB. Hence, the multimode waveguide bend we designed can solve the mode field matching problem from straight waveguide to bend waveguide. Furthermore, if the radius of bend is settled, the mode converter is suitable for bending at different angles, such as 45°, 90°, 180°, etc. For different angles of waveguide bending, the mode converter part does not need to be redesigned, but only needs to change the length of S2 part in Fig. 2(b) in the virtual space. And our design method can also be utilized for TM polarization by similar optimization process.

Figure 4(a) shows the MWB and its refractive index distribution in the virtual space, which is composited by two mode converters connected through a straight waveguide. Figure 4(b) presents the MWB in the physical space after CM, with uniform refractive index distribution in the waveguide core area. The effective radius of this MWB is 15 μm. Then we use a three-dimensional finite difference time domain (FDTD) simulation to verify its performance. Figure 5(a)–(c) show the distribution of the H_z field of the TE_0, TE_1 and TE_2 modes at the wavelength of 1550 nm respectively. The theoretical transmission spectrum of TE_0, TE_1 and TE_2 modes in the wavelength range of 1.5–1.6 μm are shown in Fig. 6 (a)-(c) respectively. The losses of TE_0, TE_1 and TE_2 modes at the wavelength of 1550 nm are 0.009 dB, 0.009 dB and 0.072 dB respectively. The inter-mode crosstalks are all lower than -28 dB. For comparison, we also simulated a traditional 180° arc-bend waveguide with the same effective radius (15 μm) and waveguide width (2 μm) as shown in Fig. 7 (a)-(c). The losses of the three lowest-order TE modes are 0.201 dB, 2.093 dB and 2.119 dB at wavelength of 1550 nm. The crosstalks of the first-order mode and the second-order mode are both higher than -4.6 dB. Thus, our design method can achieve a compact MWB with low loss and low inter-mode crosstalk.

Optics EXPRESS

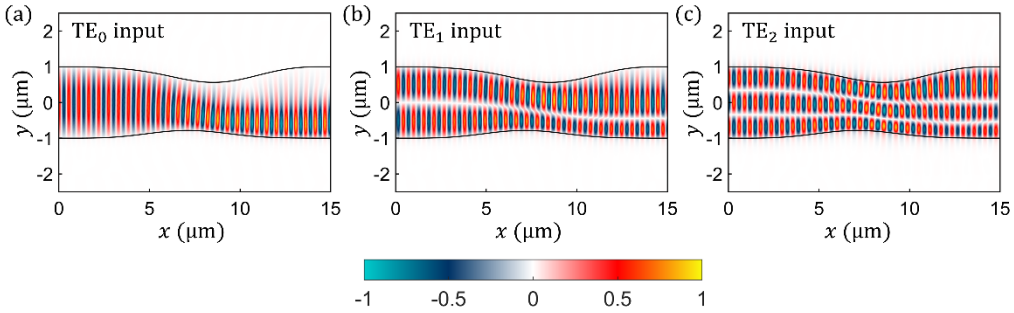

Fig. 3. The multimode transmission performances of shape-optimized mode converter in virtual space. (a)–(c) respectively show the H_z field component distribution of (a) TE_0, (b) TE_1, and (c) TE_2 modes at the wavelength of 1550 nm.

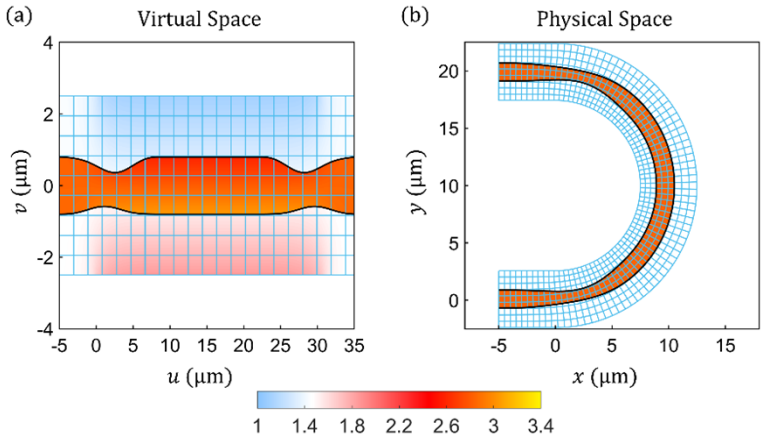

Fig. 4. The structure and refractive index distribution of shape-optimized 180° multimode waveguide bend (MWB) in (a) virtual space and (b) physical space.

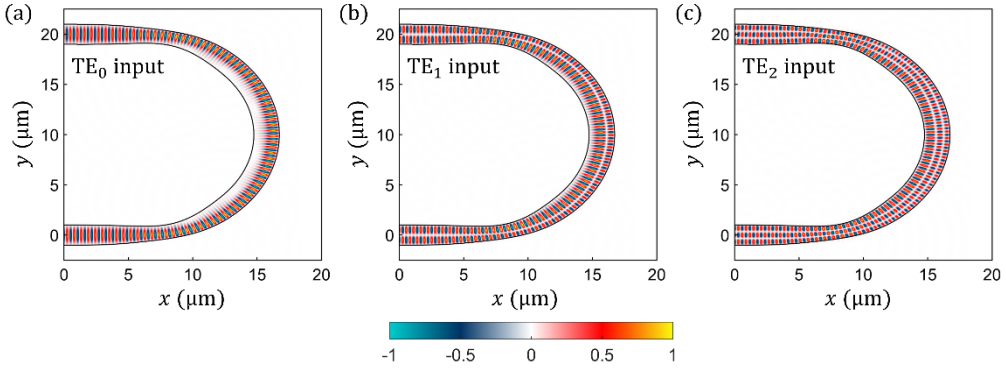

Fig. 5. Three-dimensional FDTD simulation results of 180° MWB in physical space. (a)-(c) The distribution of the H_z field of the TE_0 (a), TE_1 (b), and TE_2 (c) modes at the wavelength of 1550 nm.

Optics EXPRESS

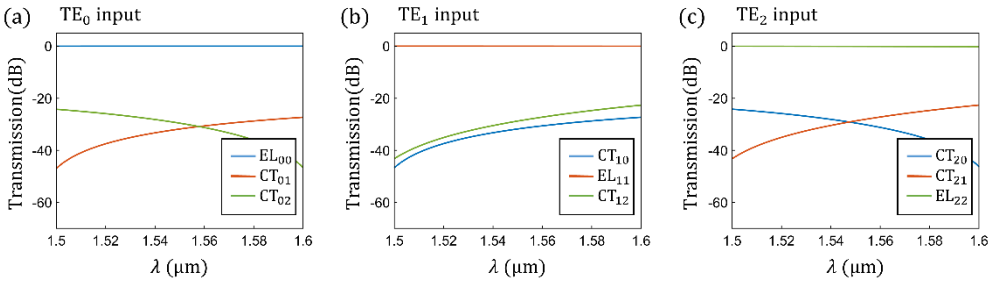

Fig. 6. The simulated transmission spectrum of 180° MWB in physical space for (a) TE_0, (b) TE_1, and (c) TE_2 modes respectively.

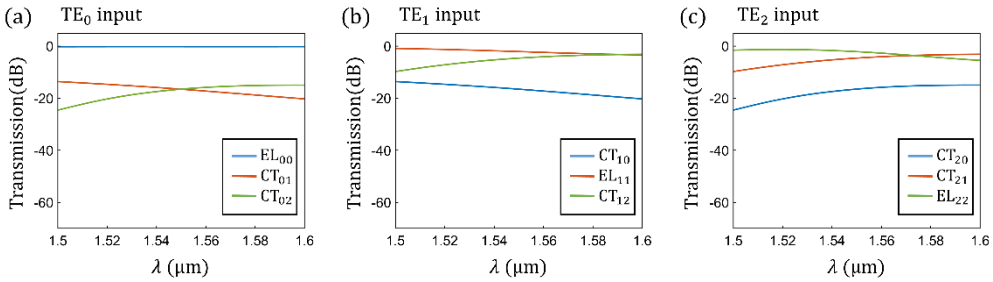

Fig. 7. The simulated transmission spectrum of a traditional 180°-arc bending waveguide with the same effective radius (15 μm) and waveguide width (2 μm). (a)-(c) show the transmission spectrum of TE_0 (a), TE_1 (b) and TE_2 (c) modes respectively.

Next, we connect two 180° MWBs with two straight multimode waveguides to form an MMRR. To selectively excite each mode in the ring resonator, the coupling region must be designed carefully to avoid inter-mode crosstalk. A bending directional coupler (BDC) is used to excite the TE_0 mode, which consists of a narrow access bending waveguide and a wide bending waveguide in the MMRR. The widths of the two bending waveguides are determined according to the bending phase-matching condition $n_{eff}R = n'_{eff}R'$ (R and R' are the bending radii of the wide bending waveguide and the access bending waveguide, n_{eff} and n'_{eff} are their effective indices for the TE_0 modes). The evanescent field coupling between the two bending waveguides is weak since the waveguide width of MMRR is as large as 2 μm. To excite the TE_0 mode sufficiently, the gap between the two bending waveguides is set to be 200 nm and the length of the BDC is the arc length of MWB excluding the mode converters. The width of the narrow access waveguide is optimized to be w = 550 nm to get the largest power coupling ratio of 0.0241. In this case, the excitement of other higher-order modes is also well suppressed.

To excite the TE_1 and TE_2 modes in the resonator selectively, we can use ADCs along the straight waveguide in MMRR. The ADCs are designed by the phase-matching condition $n_{eff} = n'_{eff}$, where n_{eff} is the effective indices for the TE_0 modes of narrow access waveguide and n'_{eff} is the effective indices for the TE_1 or TE_2 modes of wide waveguide. To ensure sufficient coupling efficiency for the TE_1 mode, the coupling length is 32 μm and the gap is 150 nm. The optimal width of the narrow waveguide of TE_1 mode ADC is 950 nm. And the power coupling ratio of the TE_1 mode is 0.0135 at 1550 nm. For the TE_2 mode ADC, the coupling length is 20 μm, the gap is 200 nm. The optimal width of the narrow access waveguide of TE_2 mode ADC is 650 nm. The power coupling ratio is 0.0229 at 1550 nm. Thus, the length of the straight waveguide in the MMRR is set to be 45 μm to accommodate the two ADCs.

Optics EXPRESS

3. Fabrication and measurement of the MMRR

The proposed MMRR was fabricated on the commercial SOI wafers with silicon core layer thickness of 220 nm and buried oxide (BOX) layer thickness of 3 μm. Only simple one-step electron beam lithography (EBL) and inductively coupled plasma (ICP) etching are needed to fabricate the MMRR. A 2 μm thick silicon dioxide layer was deposited by plasma-enhanced chemical vapor deposition (PECVD) as the upper cladding layer. Figure 8(a) shows the micrograph of the fabricated MMRR. Figure 8(b) is the zooming-in micrographs of TE_0, TE_1, and TE_2 mode couplers. Grating couplers are used to couple the light in and out between the single-mode fiber and the MMRR chip.

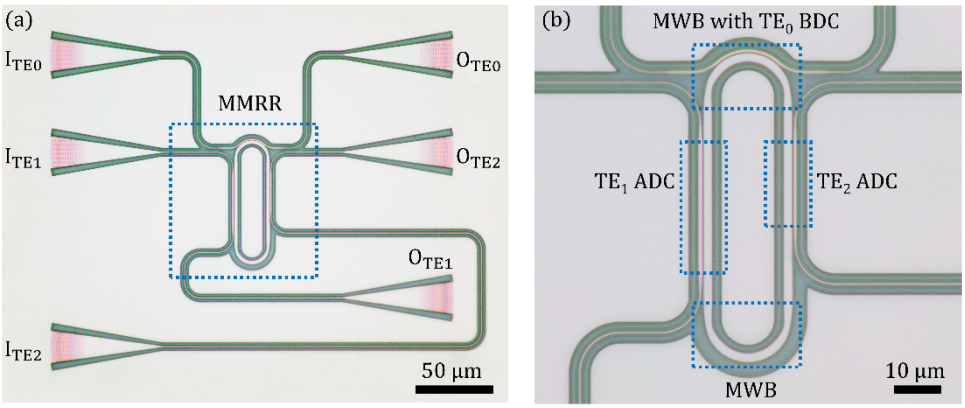

Fig. 8. (a) The microscope image of fabricated MMRR. (b) The zooming-in micrographs of TE_0 bend directional coupler, TE_1 asymmetrical directional coupler, and TE_2 asymmetrical directional coupler.

We used the broadband amplified spontaneous emission (ASE) source and the optical spectrum analyzer (OSA) to measure the resonance spectrum of each mode in the fabricated MMRR. After the output fiber, a commercial 3 dB Y-splitter is connected to split the output light into two paths. One is linked to the optical power meter for monitoring power and tuning the alignment between the single-mode fibers and the grating couplers. The other is connected to the OSA to measure the resonance spectrum for each mode. To obtain the resonance spectrum accurately, the losses of the vertical grating couplers should be deducted from the measured spectrum of the photonics integrated circuit (PIC). This can be easily realized by measuring and subtracting the transmission spectra of the PIC with and without MMRR.

Figure 9(a)-(c) shows the measured MMRR spectrum of each mode at the through ports, of which one major peak marked by a dashed circle is selected to calculate the loaded Q factor. Figure 9(d)-(f) shows the marked major peak of each mode fitted by the theoretical Lorentz curve. Based on the curve fitting, the calculated loaded Q factors are 5.9×10^4, 4.5×10^4 and 4.7×10^4 for TE_0, TE_1 and TE_2 modes at the resonant wavelength of 1551.0 nm, 1549.9 nm and 1552.0 nm respectively. Furthermore, the minor resonance peaks caused by the inter-mode crosstalk are all well suppressed compared with the major resonance peaks, which is consistent with the theoretical analysis and the simulation results of our MWB. Thus, all modes in the MMRR have achieved high Q factor with low inter-mode crosstalk. Meanwhile, the FSRs of TE_0, TE_1 and TE_2 modes are 3.7 nm, 3.6 nm and 3.4 nm respectively, which is adequate large owing to the short resonator length of MMRR. These large FSRs are very important for some applications like bio-sensing.

Optics EXPRESS

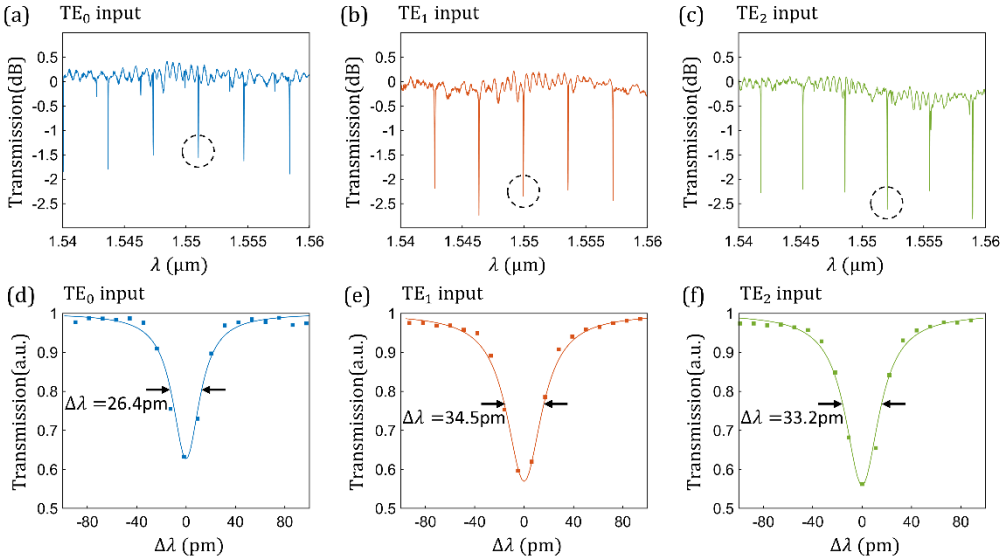

Fig. 9. (a)-(c) shows the experimental spectrum of the fabricated MMRR for TE_0 (a), TE_1 (b) and TE_2 (c) mode respectively, of which one major peak marked by the dashed circle is used to calculate the loaded Q factor. (d)-(f) shows the marked major peak fitted by the theoretical Lorentzian curve for TE_0 (d), TE_1 (e) and TE_2 (f) mode respectively.

4. Conclusion

In summary, we have proposed and realized a compact and high-Q silicon MMRR composed of two 180° MWBs and two straight waveguides. The mode converter in MWB was designed by shape-optimized in the virtual space with transformation optics. And the MWB is compatible with BDC because of the mode adiabatic evolution between the straight and bend waveguide. The effective radius of 180° MWB is as small as 15 μm to create a compact resonator with large FSRs. Meanwhile, a BDC and two ADCs have been used so that the selective mode coupling for the three lowest order TE modes can be obtained with low inter-mode crosstalk. The fabricated MMRR has high loaded Q-factors of around 5×10^4 for the three lowest order TE modes. And the FSRs for the three modes are as large as 3.4-3.6 nm. The proposed compact and high Q silicon MMRR can play a very important role in many future multimode applications, such as on-chip MDM systems, microwave photonic filters, multi-parameter optical sensors, and multimode nonlinear optics.

Funding. National Key Research and Development Program of China (2019YFB2205202); National Natural Science Foundation of China (61975062); Innovation Fund of Wuhan National Laboratory for Optoelectronics.

Acknowledgments. We thank Dr. Cheng Zeng and the engineer Mr. Pan Li in the Center of Micro-Fabrication and Characterization (CMFC) of WNLO for the support in electron-beam lithography and ICP dry etching.

Disclosures. The authors declare no conflicts of interest.

Data availability. Data underlying the results presented in this paper are not publicly available at this time but may be obtained from the authors upon reasonable request.

References

1. L. Chrostowski and M. Hochberg, *Silicon photonics design: from devices to systems* (Cambridge University, 2015).
2. C. Sun, M. T. Wade, Y. Lee, J. S. Orcutt, L. Alloatti, M. S. Georgas, A. S. Waterman, J. M. Shainline, R. R. Avizienis, S. Lin, B. R. Moss, R. Kumar, F. Pavanello, A. H. Atabaki, H. M. Cook, A. J. Ou, J. C. Leu, Y. H. Chen, K. Asanovic, R. J. Ram, M. A. Popovic, and V. M. Stojanovic, "Single-chip microprocessor that communicates directly using light," Nature **528**(7583), 534–538 (2015).

Optics EXPRESS

3. R. Soref, "The past, present, and future of silicon photonics," IEEE J. Select. Topics Quantum Electron. **12**(6), 1678–1687 (2006).
4. D. Munk, M. Katzman, Y. Kaganovskii, N. Inbar, A. Misra, M. Hen, M. Priel, M. Feldberg, M. Tkachev, A. Bergman, M. Vofsi, M. Rosenbluh, T. Schneider, and A. Zadok, "Eight-Channel Silicon-Photonic Wavelength Division Multiplexer With 17 GHz Spacing," IEEE J. Select. Topics Quantum Electron. **25**(5), 1–10 (2019).
5. F. Horst, W. M. Green, S. Assefa, S. M. Shank, Y. A. Vlasov, and B. J. Offrein, "Cascaded Mach-Zehnder wavelength filters in silicon photonics for low loss and flat pass-band WDM (de-)multiplexing," Opt. Express **21**(10), 11652–11658 (2013).
6. X. Guan, H. Wu, Y. Shi, and D. Dai, "Extremely small polarization beam splitter based on a multimode interference coupler with a silicon hybrid plasmonic waveguide," Opt. Lett. **39**(2), 259–262 (2014).
7. H. Wu, Y. Tan, and D. Dai, "Ultra-broadband high-performance polarizing beam splitter on silicon," Opt. Express **25**(6), 6069–6075 (2017).
8. D. Dai, C. Li, S. Wang, H. Wu, Y. Shi, Z. Wu, S. Gao, T. Dai, H. Yu, and H.-K. Tsang, "10-Channel Mode (de)multiplexer with Dual Polarizations," Laser Photonics Rev. **12**(1), 1700109 (2018).
9. L. W. Luo, N. Ophir, C. P. Chen, L. H. Gabrielli, C. B. Poitras, K. Bergmen, and M. Lipson, "WDM-compatible mode-division multiplexing on a silicon chip," Nat. Commun. **5**(1), 3069 (2014).
10. S. Gao, H. Wang, X. Yi, and C. Qiu, "Ultra-compact multimode waveguide bend with shallowly etched grooves," Opt. Express **29**(23), 38683–38690 (2021).
11. W. Chang and M. Zhang, "Silicon-based multimode waveguide crossings," JPhys Photonics **2**(2), 022002 (2020).
12. S. Li, Y. Zhou, J. Dong, X. Zhang, E. Cassan, J. Hou, C. Yang, S. Chen, D. Gao, and H. Chen, "Universal multimode waveguide crossing based on transformation optics," Optica **5**(12), 1549 (2018).
13. L. Han, B. P. Kuo, N. Alic, and S. Radic, "Ultra-broadband multimode 3 dB optical power splitter using an adiabatic coupler and a Y-branch," Opt. Express **26**(11), 14800–14809 (2018).
14. C. Sun, W. Wu, Y. Yu, G. Chen, X. Zhang, X. Chen, D. J. Thomson, and G. T. Reed, "De-multiplexing free on-chip low-loss multimode switch enabling reconfigurable inter-mode and inter-path routing," Nanophotonics **7**(9), 1571–1580 (2018).
15. L. Yang, T. Zhou, H. Jia, S. Yang, J. Ding, X. Fu, and L. Zhang, "General architectures for on-chip optical space and mode switching," Optica **5**(2), 180 (2018).
16. G. Liang, H. Huang, A. Mohanty, M. C. Shin, X. Ji, M. J. Carter, S. Shrestha, M. Lipson, and N. Yu, "Robust, efficient, micrometre-scale phase modulators at visible wavelengths," Nat. Photonics **15**(12), 908–913 (2021).
17. H. Q. Qiu, F. Zhou, J. R. Qie, Y. H. Yao, X. Hu, Y. G. Zhang, X. Xiao, Y. Yu, J. J. Dong, and X. L. Zhang, "A Continuously Tunable Sub-Gigahertz Microwave Photonic Bandpass Filter Based on an Ultra-High-Q Silicon Microring Resonator," J. Lightwave Technol. **36**(19), 4312–4318 (2018).
18. P. Dong, "Silicon Photonic Integrated Circuits for Wavelength-Division Multiplexing Applications," IEEE J. Select. Topics Quantum Electron. **22**(6), 370–378 (2016).
19. B. Stern, X. Ji, A. Dutt, and M. Lipson, "Compact narrow-linewidth integrated laser based on a low-loss silicon nitride ring resonator," Opt. Lett. **42**(21), 4541–4544 (2017).
20. R. R. Singh, S. Kumari, A. Gautam, and V. Priye, "Glucose sensing using slot waveguide-based SOI ring resonator," IEEE J. Sel. Top. Quantum Electron **25**(1), 1–8 (2019).
21. L. Zhang, S. Hong, Y. Wang, H. Yan, Y. Xie, T. Chen, and D. Dai, "New-generation silicon photonics beyond the singlemode regime," arXiv preprint arXiv:2104.04239. (2021).
22. S. Li, Z. Nong, X. Wu, W. Yu, M. He, C. Klitis, Y. Zhu, S. Gao, J. Liu, Z. Li, L. Liu, M. Sorel, S. Yu, and X. Cai, "Orbital angular momentum vector modes (de)multiplexer based on multimode micro-ring," Opt. Express **26**(23), 29895–29905 (2018).
23. D. Hu, C. L. Zou, H. Ren, J. Lu, Z. Le, Y. Qin, S. Guo, C. Dong, and W. Hu, "Multi-Parameter Sensing in a Multimode Self-Interference Micro-Ring Resonator by Machine Learning," Sensors **20**(3), 709 (2020).
24. X. Lu, G. Moille, A. Rao, D. A. Westly, and K. Srinivasan, "Efficient photoinduced second-harmonic generation in silicon nitride photonics," Nat. Photonics **15**(2), 131–136 (2021).
25. B. A. Dorin and W. N. Ye, "Two-mode division multiplexing in a silicon-on-insulator ring resonator," Opt. Express **22**(4), 4547–4558 (2014).
26. Z. Chen, M. Ye, L. Zhang, Q. Zhang, H. Xie, Y.-F. Xiao, and Y. Wang, "Compact mode-insensitive ring resonator based on SWG coupler and Euler bends," Proc. SPIE **12066**, 36–149 (2021).
27. M. Ye, C. Sun, Y. Yu, Y. Ding, and X. Zhang, "Silicon integrated multi-mode ring resonator," Nanophotonics **10**(4), 1265–1272 (2021).
28. J. B. Pendry, D. Schurig, and D. R. Smith, "Controlling electromagnetic fields," Science **312**(5781), 1780–1782 (2006).
29. U. Leonhardt, "Optical conformal mapping," Science **312**(5781), 1777–1780 (2006).
30. A. Vakil and N. Engheta, "Transformation Optics Using Graphene," Science **332**(6035), 1291–1294 (2011).
31. H. Barati Sedeh, M. H. Fakheri, A. Abdolali, F. Sun, and Y. Ma, "Feasible Thermodynamics Devices Enabled by Thermal-Null Medium," Phys. Rev. Appl. **14**(6), 064034 (2020).
32. M. H. Fakheri, A. Ashrafian, H. Barati Sedeh, and A. Abdolali, "Experimental Verification of Shape-Independent Surface Cloak Enabled by Nihility Transformation Optics," Adv. Opt. Mater. **9**(19), 2100816 (2021).

Optics EXPRESS

33. F. Sun and S. He, "Optical Surface Transformation: Changing the optical surface by homogeneous optic-null medium at will," Sci. Rep. **5**(1), 16032 (2015).
34. L. Xu and H. Chen, "Conformal transformation optics," Nat. Photonics **9**(1), 15–23 (2015).
35. S. Li, L. Cai, D. Gao, J. Dong, J. Hou, C. Yang, S. Chen, and X. Zhang, "Compact and broadband multimode waveguide bend by shape-optimizing with transformation optics," Photonics Res. **8**(12), 1843 (2020).